ELSEVIER

Biophysical Chemistry 65 (1997) 29–44

Biophysical Chemistry

Influence of diffusion to fractal surfaces on the binding kinetics for antibody–antigen, analyte–receptor, and analyte–receptorless (protein) systems

Ajit Sadana *, Milind Sutaria

Chemical Engineering Department, University of Mississippi, University, MS 38677-9740, USA

Received 25 September 1995; revised 23 October 1996; accepted 29 October 1996

Abstract

The diffusion-limited binding kinetics of antigen–antibody, ligand–receptor, analyte–receptorless systems for biosensor applications is analyzed within a fractal framework. The analysis presented applies equally well to these types of systems. For example, for the binding of 2-(*p*-toluidinyl)-naphthalene-6-sulfonic acid (2,6-TNS) to β-cyclodextrin (ligand–receptor system) immobilized on a fiber-optic base inclusate biosensor, an increase in temperature from 4 to 30°C leads to an increase in the fractal dimension, D_f and to a decrease in the binding rate coefficient, k_1. For the binding of TRITC-labeled low-density proteins (LDL) directly to an optical fiber-based sensor (analyte–receptorless system), an increase in the LDL concentration from 5 to 50 $\mu g\ ml^{-1}$ in solution leads to a decrease in the fractal dimension, D_f and to an increase in the binding rate coefficient, k_1. Also, during the binding of human chorionic gonadotropin (hCG) to anti-hCG antibody immobilized on a HPLC column (antigen–antibody system), an increase in temperature from 4 to 50°C leads to an increase in the fractal dimension, D_f and in the binding rate coefficient, k_1. The different examples analyzed and presented together for the three different types of systems provide one means of a 'unified analysis,' and a method by which the forward binding rate coefficient, k_1 may be controlled, that is, by changing the fractal dimension or 'disorder' on the surface. The analysis should assist in improving the stability, sensitivity, and response time of biosensors wherein different types of binding systems are utilized in the analysis method. More-or-less all of the treatment presented should be applicable to the above types of binding systems occurring in non-biosensor applications also. However, the single-fractal analysis is unable to describe the data over the full time course of some of the experiments. © 1997 Elsevier Science B.V.

Keywords: Antibody–antigen, analyte–receptor, and analyte–receptorless (protein) systems; Binding kinetics; Diffusion; Fractal surfaces

1. Introduction

The diffusive motion of reactants to irregular surfaces exhibit dispersive behavior and can play an important role in determining the rate of reactions occurring at surfaces. Some of the typical reactions include antigen–antibody for biosensor applications, cell-receptor reactions occurring on membrane surfaces, and protein adsorption reactions for biomedical applications. Seri-Levy and Avnir [1] emphasize that a large proportion of surfaces in nature exhibit fractal characteristics. Furthermore, fractal approaches are being applied more and more in inter-

* Corresponding author.

0301-4622/97/$17.00 Copyright © 1997 Elsevier Science B.V. All rights reserved.
PII S0301-4622(96)02253-3

face science [2]. Seri-Levy and Avnir [1] indicate that a fractal analysis provides unique insights relating the nature of the surface with the 'activity' of the reactant either adsorbed directly to the surface or bound to an appropriate 'receptor' on the surface. Pajkossy and Nyikos [3] indicate that the fractal approach provides a very efficient way of characterizing irregularity in very general terms. Goetze and Brickmann [4] emphasize that a large number of systems in nature exhibit self-similar characteristics, ranging from molecular protein systems all the way up to astrophysical systems. Glockle and Nonenmacher [5] have recently emphasized that scaling laws and self-similar behavior are fundamental features of complex systems.

Antigen–antibody binding kinetics for biosensor applications have been analyzed using a fractal approach [6–10]. Fresh physical insights were obtained. For example, the binding rate coefficient and the rate of binding was linked to the fractal dimension, or the degree of surface roughness. The above mentioned fractal analysis is of a general nature, and more-or-less all of the treatment can presumably be extended to apply to any receptor–ligand model or analyte–receptorless system.

Low-dimension fractals have been observed for analyte–receptorless systems, for example, during the computer-simulated aggregation of ferritin [11], the adsorption of ferritin on a quartz surface [12], and polymer adsorption [13]. A fractal analysis has been utilized to examine the binding of pyrene (ligand) in solution to β-cyclodextrin (receptor) immobilized on a fiber-optic biosensor [14]. These authors were able to come up with a predictive equation for the fractal dimension with respect to the pyrene concentration in solution. For receptor–ligand systems it is recognized that the population of receptors for a given ligand may be represented by several subpopulations with different affinities [15–18]. Jose [19] has developed a model for ligand binding systems at equilibrium, and has analyzed the influence of heterogeneity, cross-reactivity, and site–site interactions on this system. Site–site interactions are themselves a source of affinity heterogeneity [20], and their binding to different types of ligands may effectively be described by fractal systems. Swalen et al. [21] have indicated that the control of the structural organization of molecules at an interface are a key to understanding the reactions at interfaces and for the design of advanced materials. The characterization of a solid surface for antibody–antigen, receptor–ligand, and analyte–receptorless binding systems is of immediate importance [22]. Losche et al. [23] have recently analyzed the influence of surface chemistry on the adsorption of protein layers on aqueous interfaces and structural organization. Axelrod and Wang [24] have indicated the importance of reduction of dimensionality kinetics, wherein reactions between ligands and cell surface receptors can be enhanced by non-specific adsorption followed by two-dimensional diffusion to a cell-surface receptor.

In this manuscript, we extend the fractal analysis of the binding kinetics of antibody–antigen for biosensor applications [8,9] to ligand–receptor and to analyte–receptorless systems with the intent to develop the steps towards a 'unified approach' to help characterize these types of systems. We intend to analyze and to search for 'similarities', if any, that may occur during the fractal analysis of these 'similar' types of biochemical systems occurring at

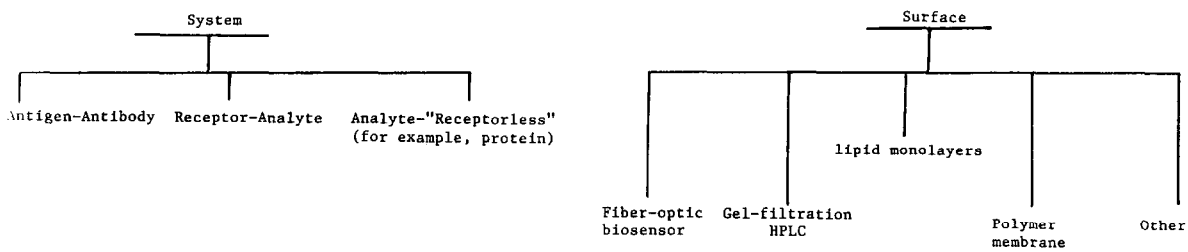

Fig. 1. Some possible binding scenarios (system + surface = process).

solid–liquid interfaces. Fig. 1 indicates the scope of the work or types of systems we intend to characterize using the fractal analysis.

2. Theory

An analysis of the binding kinetics of antigen in solution to an antibody immobilized on the biosensor surface is available [25,26]. The influence of lateral interactions on the surface and variable rate coefficients is also available [6]. Fractal dimension values have been obtained for antibody–antigen binding systems for biosensor applications [8,9] and for a single case of a ligand–receptor system [14]. Here, we attempt to extend the above mentioned ideas and concepts from antigen–antibody binding kinetics to also include analyte (ligand)–receptor binding (more examples are now presented), and to the binding of the analyte directly to the surface ('receptorless'), for example protein adsorption. This will be done for biosensor applications. More-or-less, however, the treatment is also applicable to the different binding cases for non-biosensor applications.

2.1. Variable binding rate coefficient

Kopelman [27] has recently indicated that classical reaction kinetics is sometimes unsatisfactory when the reactants are spatially constrained on the microscopic level by either walls, phase boundaries, or force fields. Such heterogeneous reactions, for example, bioenzymatic reactions, that occur at interfaces of different phases exhibit fractal orders for elementary reactions and rate coefficients with temporal memories. In such reactions, the rate coefficient exhibits a form given by:

$$k_1 = k' t^{-b} \quad 0 < b < 1 (t > 1) \tag{1a}$$

In general, k_1 depends on time, whereas $k' \propto k_1(t = 1)$ does not. Kopelman [27] indicates that in three dimensions (homogeneous space), b equals zero. This is in agreement with the results obtained in classical kinetics. Also, with vigorous stirring, the system is made homogeneous and b again equals zero. However, for diffusion-limited reactions occurring in fractal spaces, $b > 0$; this yields a time-dependent rate coefficient.

The random fluctuations on a two-state process in ligand binding kinetics has been analyzed [28]. The stochastic approach can be used as a means to explain the variable binding rate coefficient. The simplest way to model these fluctuations is to assume that the binding rate coefficient $k_1(t)$ is the sum of its deterministic value (invariant) and the fluctuation ($z(t)$) [28]. This $z(t)$ is a random function with a zero mean. The decreasing and increasing binding rate coefficients can be assumed to exhibit an exponential form [6,29,30]:

$$k_1 = k_{1,0} \exp(-\beta t)$$

$$k_1 = k_{1,0} \exp(\beta t) \tag{1b}$$

Here, β and $k_{1,0}$ are constants.

Sadana and Madagula [6] have analyzed the influence of a decreasing and an increasing binding rate coefficient on the antigen concentration near the surface when the antibody is immobilized on the surface. The authors noted that for an increasing binding rate coefficient, after a brief time interval, as time increases, the concentration of the antigen near the surface decreases, as expected for the cases when lateral interactions are present or absent. The diffusion-limited binding kinetics of antigen (or antibody or substrate) in solution to antibody (or antigen or enzyme) immobilized on a biosensor surface has been analyzed within a fractal framework [8,31]. Furthermore, experimental data presented for the binding of HIV virus (antigen) to the antibody anti-HIV immobilized on a surface displays a characteristic ordered 'disorder' [32]. This indicates the possibility of a fractal-like surface. There are sufficient similarities between antigen–antibody, ligand–receptor, and analyte–'receptorless' systems that one may attempt to extend the fractal analysis utilized for antigen–antibody systems to ligand–receptor and analyte–receptorless systems.

The diffusion of reactants toward fractal surfaces has been analyzed [33–36]. Havlin [37] briefly reviewed and discussed the results, and Sadana and coworkers [7,9] have utilized fractals to analyze antigen–antibody binding systems for biosensor applications. We will use the words ligand–receptor as the generic term to represent antibody–antigen, ligand–receptor, and analyte–receptorless (protein adsorption) systems.

Havlin [37] indicates that the diffusion of a particle (ligand) from a homogeneous solution to a solid surface (receptor coated biosensor surface), where it reacts to form a product (ligand–receptor complex, ligand.receptor) is given by:

$$(\text{ligand.receptor}) \sim \begin{cases} t\dfrac{(3-D_f)}{2} = t^p & t < t_c \\ t^{1/2} & t > t_c \end{cases} \quad (2)$$

Here, D_f is the fractal dimension of the surface. Eq. (2) indicates that the concentration of the product, [ligand.receptor](t) in the reaction ligand + receptor → (ligand.receptor) on a solid surface scales as $[(\text{ligand.receptor})](t) \sim t^p$, with the coefficient $p = (3 - D_f)/2$ at short time scales and $p = 1/2$ at intermediate time scales. This equation is associated with the short-term diffusional properties of a random walk on a fractal surface. Note that, in perfectly stirred kinetics on a regular (non-fractal) structure (or surface), k_1 is constant, that is, it is independent of time. In other words, the limit of regular structures (or surfaces) and the absence of diffusion-limited kinetics lead to k_1 being independent of time. In all other situations, one would expect scaling behavior given by $k_1 \sim k' t^{-b}$ with $-b = p < 0$. Also, the appearance of the coefficient p different from $p = 0$ is the consequence of two different phenomena, that is, the heterogeneity (fractality) of the surface and the imperfect mixing (diffusion-limited conditions). Havlin [37] indicates that the crossover value may be determined by $r_c^2 \sim t_c$. Above the characteristic length, r_c, the self-similarity of the surface is lost. Above r_c, the surface may be considered homogeneous, since the self-similarity property disappears and regular diffusion is now present. One may consider the analysis to be presented as an intermediate heuristic approach, in that in the future one may also be able to develop an autonomous (and not time-dependent) model of diffusion-controlled kinetics in disordered media.

3. Results

We now analyze the influence of different parameters on the binding kinetics of ligand–receptor systems within a fractal framework.

3.1. Effect of temperature: increase in the fractal dimension with temperature

Litwiler et al. [38] have developed a fiber-optic-base inclusate sensor (FOBIS) utilizing β-cyclodextrin (β-CD) immobilized on a surface which acts as the receptor for the analyte or ligand, 2-(*p*-toluidinyl)naphthalene-6-sulfonic acid (2,6-TNS). These authors indicate that fluorescence is enhanced by inclusion complexation of quite a few fluorophores with β-CD. Litwiler et al. [38] indicate that the inclusion of the analyte or ligand in the β-CD cavity protects it from bulk solution quenchers such as water. This is because the inclusate is in a more hydrophobic environment. Furthermore, these authors indicate that the sensitivity and selectivity are significantly dependent on the analyte geometry and functional group orientation, in other words on the extent of surface roughness. Thus, this is a very viable candidate for fractal analysis.

Fig. 2 shows the binding (increase in fluorescence) of 2,6-TNS (100 nM injections) to β-cyclodextrin at different temperatures ranging from 4 to 30°C, with the results of the model regression derived from the fractal approach [7]. In all of the figures, a solid line shows the fit of the model (Eq. (2)) to the experimental data available in the literature. Table 1 shows the values of the parameters, k_1, p, and the fractal dimension, D_f obtained using Eq. (2), a biphasic function of time, to model the experimental data for the binding of 2,6-TNS to β-cyclodextrin immobilized on the surface. The binding rate coefficient, k_1, value presented in Table 1 was obtained from a regression analysis using Sigmaplot [43] to model the experimental data using Eq. (2), wherein $(\text{ligand.receptor}) = k_1 t^p$. The k_1, p, and D_f values presented in Table 1 are within 95% confidence limits. For example, the value of k_1 reported for the binding of 100 nM 2,6-TNS is 1.8051 ± 0.133. The 95% confidence limits indicates that 95% of the k_1 values will fall between 1.9381 and 1.6721. This indicates that the values are precise and significant.

Table 1 shows that D_f increases from 1.984 to 2.753 as the temperature increases from 4 to 30°C. In this same temperature range the binding rate coefficient, k_1 decreases from 7.861 to 1.805. An increase in temperature from 4 to 30°C leads to an increase in

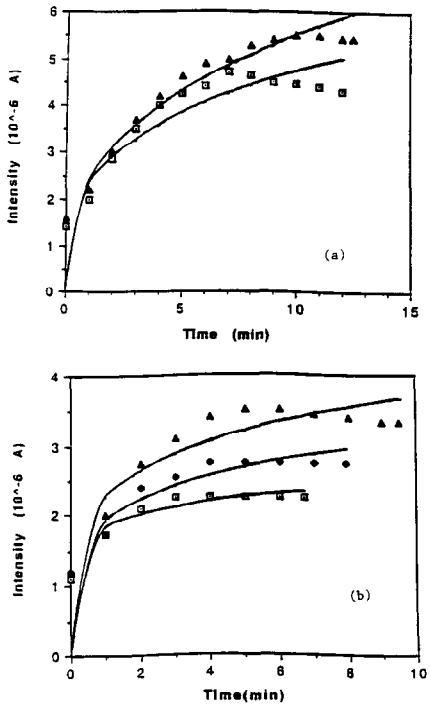

Fig. 2. Binding rate curves (increase in fluorescence) for 2,6-TNS in solution to β-cyclodextrin immobilized on a fiber-optic base inclusate sensor (FOBIS) at different temperatures (°C) [38]: (a) ▲ 10; □ 15, (b) ▲ 20; ◆ 25; □ 30.

the fractal dimension by 38.7%, and to a decrease in the binding rate coefficient, k_1 by 77%. The changes in the fractal dimension and in the binding rate coefficient are in opposite directions.

More refined fits (that would minimize or eliminate the systematic deviation) could have been obtained if a multi-fractal analysis instead of a single-fractal analysis was used (as and when required) to model the data in Fig. 2 and for other data analysis to be presented in later figures. Multi-fractal dimensions have been indicated in adsorption [2], and for other systems [44]. Such an analysis is not presented here since for the present, based on the current state of knowledge, we feel that a single fractal analysis is sufficient to adequately describe ligand–receptor kinetics for the biosensor systems analyzed.

In the case of Fig. 2, a dual-fractal analysis would help capture the maximum exhibited, which the single fractal analysis is unable to do. The dual-fractal analysis would also suggest a change in the state of disorder or degree of heterogeneity on the surface caused by a change in the mechanism such as a change in fluorescence response of the biosensor or a desorption. Fitting the data by a single fractal analysis vis-a-vis a dual-fractal analysis does bias the parameters to some extent.

Note also that the model as presented passes through the origin, even though the data is at 1.5 at time, t equal to zero (for example, see Fig. 2a). This is intuitively correct as far as the model is concerned. The inability of the model to describe early time data may be attributed to inadequate experimental procedure leading to unreliable early time data since no clue for this is available in the original paper. For example, no information is provided about a background signal. Nevertheless, we add that the present model is unable to describe the data over the full time course of the experiment.

Fig. 3 indicates that there is a linear increase and a linear decrease in the D_f and k_1 values, respectively, with increasing temperature from 4 to 30°C. More experimental data would more firmly establish the trends presented. The decrease in the binding rate coefficient with increase in temperature is due to the system utilized for immunochemical analysis.

Nakamura et al. [39] have recently developed a liquid-phase assay for human chorionic gonadotropin (hCG) using high-performance liquid chromatography. They used this system to analyze liquid-phase antigen–antibody reactions. Anti-hCG monoclonal antibodies were selected and immobilized on a Shimadzu Model LC-6A HPLC system. These antibodies recognize different hCG epitopes. The immunoreactions were carried on the column using 110 pM hCG solutions within a temperature range from 4 to 50°C. Fig. 4 depicts the kinetic data for hCG binding, with the results of the model regression derived from the fractal approach. Table 1 shows that as the temperature increases from 4 to 50°C the fractal dimension, D_f increases from 1.983 to 2.526, and the binding rate coefficient, k_1 increases from 7.861 to 15.47. In this case an increase in temperature from 4 to 50°C, leads to changes in the D_f and in the k_1 values in the same direction. An increase in the fractal dimension by 27.3% leads to an increase in the binding rate coefficient by 97%.

Clearly, a dual-fractal analysis would once again provide a more refined fit by minimizing or eliminat-

Table 1
Influence of different parameters on the fractal dimension, D_f, and on the binding rate coefficient, k_1

Antibody or receptor concentration	Antigen or analyte concentration	Surface for immobilization	k_1	p	D_f	Ref.
Effect of temperature						
β-Cyclodextrin (β-CD)	2-(*p*-Toluidinyl)-naphthalene-6-sulfonic acid (2,6-TNS) 100 nM, 30°C	Silica-immobilized β-CD attached to distal end of a bifurcated fiber-optic probe	1.8051 ± 0.133	0.1236 ± 0.0285	2.753 ± 0.057	[38]
β-CD	100 nM 2,6-TNS, 25°C	Same as above	1.933 ± 0.143	0.2036 ± 0.0385	2.593 ± 0.077	[38]
β-CD	100 nM 2,6-TNS, 20°C	Same as above	2.285 ± 0.211	0.2113 ± 0.04	2.5774 ± 0.081	[38]
β-CD	100 nM 2,6-TNS, 15°C	Same as above	2.3344 ± 0.2583	0.3081 ± 0.042	2.3839 ± 0.084	[38]
β-CD	100 nM 2,6-TNS, 10°C	Same as above	2.3978 ± 0.151	0.3616 ± 0.023	2.2768 ± 0.0463	[38]
Anti-hCG monoclonal antibody	110 pM hCG, 4°C	Gel filtration high-performance liquid chromatography column	7.861 ± 1.101	0.5082 ± 0.0219	1.9836 ± 0.0438	[39]
Anti-hCG monoclonal antibody	110 pM hCG, 30°C	Same as above	11.66 ± 1.220	0.5625 ± 0.0635	1.875 ± 0.1270	[39]
Anti-hCG monoclonal antibody	110 pM hCG, 37°C	Same as above	10.29 ± 1.222	0.5496 ± 0.0733	1.9008 ± 0.1466	[39]
Anti-hCG monoclonal antibody	110 pM hCG, 50°C	Same as above	15.47 ± 1.184	0.2369 ± 0.052	2.5262 ± 0.124	[39]
Effect of non-specific binding (or adsorption)						
Anti-fluorescein monoclonal antibody 4-4-20	10 mol% DODA-$(ED)_4$-FITC in 90 mol% POPC	Fluoresceinated lipids incorporated into lipid monolayers	0.00448 ± 0.0002	0.8305 ± 0.2414	1.3391 ± 0.4829	[40]
Anti-fluorescein monoclonal antibody 4-4-20	Pure POPC	Lipid monolayer (non-specific binding)	0.00873 ± 0.0008	0.3421 ± 0.0499	2.3158 ± 0.099	[40]
Effect of concentration						
Anti-hCG monoclonal antibody	11 pM hCG	Gel filtration high-performance liquid chromatography column	1.1198 ± 0.2113	0.4424 ± 0.0793	2.1152 ± 0.1585	[39]
Anti-hCG monoclonal antibody	28 pM hCG	Same as above	5.025 ± 1.619	0.4024 ± 0.1339	2.1952 ± 0.2678	[39]
Anti-hCG monoclonal antibody	55 pM hCG	Same as above	11.99 ± 2.294	0.3458 ± 0.084	2.3084 ± 0.168	[39]
Anti-hCG monoclonal antibody	110 pM hCG	Same as above	22.48 ± 6.031	0.3257 ± 0.114	2.3486 ± 0.2280	[39]
Anti-hCG monoclonal antibody	220 pM hCG	Same as above	49.11 ± 10.31	0.1900 ± 0.0914	2.620 ± 0.1828	[39]
Anti-hCG monoclonal antibody	548 pM hCG	Same as above	93.51 ± 10.94	0.07591 ± 0.053	2.8482 ± 0.106	[39]

500 mg ml^{-1} of 1:1 mixture of anti-phenatoine and anti-lidocaine	0 mg ml^{-1} phenatoine	Fiber optic surface	10.88 ± 0.626	0.4424 ± 0.0284	2.116 ± 0.057	[41]
500 mg ml^{-1} of 1:1 mixture of anti-phenatoine and anti-lidocaine	0.2 mg ml^{-1} phenatoine	Fiber optic surface	6.449 ± 0.2517	0.4459 ± 0.0191	2.108 ± 0.0382	[41]
500 mg ml^{-1} of 1:1 mixture of anti-phenatoine and anti-lidocaine	0.02 mg ml^{-1} phenatoine	Fiber optic surface	6.233 ± 0.135	0.4896 ± 0.0109	2.02 ± 0.0218	[41]
500 mg ml^{-1} of 1:1 mixture of anti-phenatoine and anti-lidocaine	2 mg ml^{-1} phenatoine	Fiber optic surface	6.8021 ± 0.149	0.4005 ± 0.0112	2.200 ± 0.0224	[41]
500 mg ml^{-1} of 1:1 mixture of anti-phenatoine and anti-lidocaine	20 mg ml^{-1} phenatoine	Fiber optic surface	8.839 ± 0.337	0.2728 ± 0.1899	2.456 ± 0.378	[41]
500 mg ml^{-1} of 1:1 mixture of anti-phenatoine and anti-lidocaine	0 mg ml^{-1} lidocaine	Fiber optic surface	9.741 ± 0.830	0.5213 ± 0.0735	1.958 ± 0.1468	[41]
500 mg ml^{-1} of 1:1 mixture of anti-phenatoine and anti-lidocaine	0.02 mg ml^{-1} lidocaine	Fiber optic surface	6.750 ± 0.845	0.5581 ± 0.0796	1.884 ± 0.154	[41]
500 mg ml^{-1} of 1:1 mixture of anti-phenatoine and anti-lidocaine	0.2 mg ml^{-1} lidocaine	Fiber optic surface	4.354 ± 0.371	0.6023 ± 0.0550	1.796 ± 0.163	[41]
500 mg ml^{-1} of 1:1 mixture of anti-phenatoine and anti-lidocaine	2 mg ml^{-1} lidocaine	Fiber optic surface	3.159 ± 0.0319	0.6243 ± 0.0216	3.1591 ± 0.0319	[41]
500 mg ml^{-1} of 1:1 mixture of anti-phenatoine and anti-lidocaine	20 mg ml^{-1} lidocaine	Fiber optic surface	4.268 ± 0.0500	0.5224 ± 0.0337	1.956 ± 0.0674	[41]
Lipophilic anionic sites on a di-tert-butyl-0,0′-*bis*-(2,2-dichlorovinyl)-tartarate (DBVT)	0.1 mM thiamine	Plasticized polymer membrane	0.02942 ± 0.0041	1.1913 ± 0.1325	0.6174 ± 0.1325	[26]
Lipophilic anionic sites on DBVT	1 mM thiamine	Plasticized polymer membrane	0.7645 ± 0.1165	0.4047 ± 0.0845	2.1906 ± 0.1690	[26]
Lipophilic anionic sites on DBVT	3 mM thiamine	Plasticized polymer membrane	1.6834 ± 0.1155	0.1653 ± 0.0395	2.6694 ± 0.0790	[26]
Lipophilic anionic sites on DBVT	10 mM thiamine	Plasticized polymer membrane	1.574 ± 0.354	0.3735 ± 0.1211	2.2530 ± 0.2420	[26]
Lipophilic anionic sites on DBVT	100 mM thiamine	Plasticized polymer membrane	2.621 ± 0.168	0.3188 ± 0.0370	2.3625 ± 0.0739	[26]
Receptorless surface; direct adsorption	5 $\mu g\ ml^{-1}$ TRITC-labeled low-density lipoprotein (LDL)	Optical fiber-based biosensor	122.452 ± 2.541	0.1298 ± 0.0082	2.7404 ± 0.0164	[42]
Receptorless surface; direct adsorption	10 $\mu g\ ml^{-1}$ TRITC-labeled LDL	Optical fiber-based biosensor	175.95 ± 2.825	0.1758 ± 0.0049	2.6484 ± 0.0098	[42]
Receptorless surface; direct adsorption	50 $\mu g\ ml^{-1}$ TRITC-labeled LDL	Optical fiber-based biosensor	263.22 ± 7.056	0.2085 ± 0.0119	2.5829 ± 0.0238	[42]

ing the systematic deviation for all of the four temperatures (4, 30, 37, and 50°C) in Fig. 4. k_1 and D_{f1} may be utilized to model the initial region, and the latter part of the binding curve may be modelled using a different value of the binding rate coefficient, k_2, and the fractal dimension, D_{f2}. Note that the value of p obtained (slope of the binding rate curve) at later times (p_2) decreases when compared to the value of p obtained at earlier times (p_1). This indicates that the state of disorder or the fractal dimension value would increase (since $p = (3 - D_f)/2)$) as the reaction progresses on the reaction surface. Once again, one must add that the model is unable to describe the data over the full time course of the experiment.

Fig. 5 shows that as the temperature increases from 4 to 50°C, the binding rate coefficient, k_1 increases linearly. More data points would more firmly establish this trend. The fractal dimension, D_f exhibits a minimum value around 29°C. After about

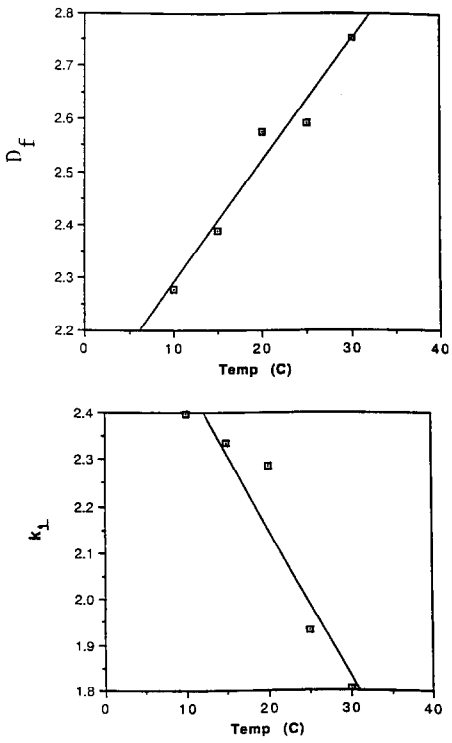

Fig. 3. Linear increase and decrease in D_f and in k_1, respectively, with temperature for the binding of 2,6-TNS to β-cyclodextrin immobilized on a FOBIS sensor [38].

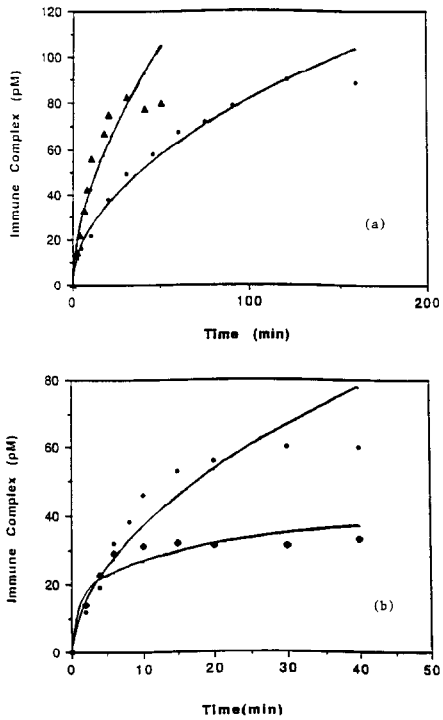

Fig. 4. Binding rate curves for human chorionic gonadotropin (hCG) to anti-hCG immobilized on a HPLC column using a liquid phase assay at different temperatures (°C) ([39]: (a) ● 37; ▲ 50; ◆ 4; ● 30.

35°C there is relatively a rapid rise in the fractal dimension as temperature increases to 50°C. Once again, the availability of more data points would more firmly establish the shape of the curve. At present, no explanation is offered for the 'weak' minimum exhibited around 29°C.

3.2. Effect of non-specific binding

Ahlers et al. [40] have recently analyzed the quenching behavior of fluorescein-conjugated lipids by antibodies. These authors indicate that antibody recognition of cell-surface antigens in a membrane surface are essential to understanding histocompatible and immune response behavior. Fluoresceinated lipids were incorporated into lipid monolayers. The anti-fluorescein antibody recognized and quenched the antigen on the surface. Fig. 6 shows the fit of the model for the specific binding of anti-fluorescein antibody to a mixed monolayer of 10 mol% 1-*N*,*N*-

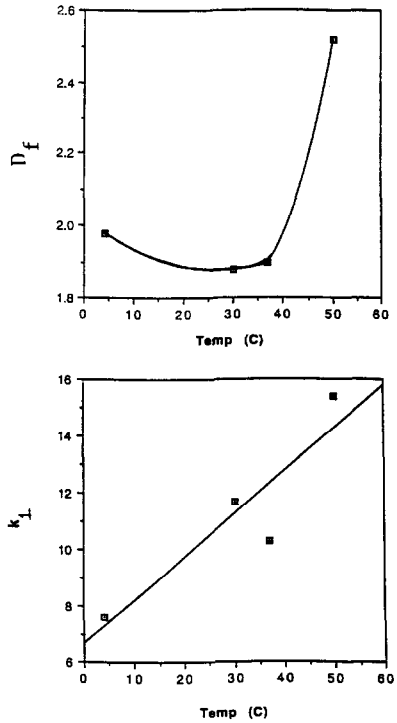

Fig. 5. Linear increase in the binding rate coefficient, k_1 and changes in the fractal dimension, D_f with temperature [39].

dioctadecylamidocarboxy-19-(5′-fluorescein thioureoyl-4-carboxy-5-oxa-2,8,11,14,17-pentaoxanonadecane (DODA-$(EO)_4$-FITC) and 90 mol% 1-α-phosphatidylcholine, β-oleoyl-γ-palmitoyl (POPC). The

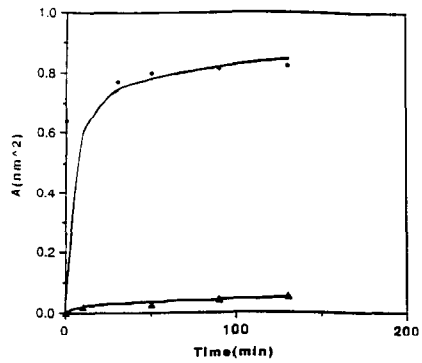

Fig. 6. Binding rate curves for anti-fluorescein antibody to 10 mol% DODA and 90 mol% POPC (specific binding), and to pure POPC (non-specific binding) [40]. ● Specific binding; ▲ non-specific binding.

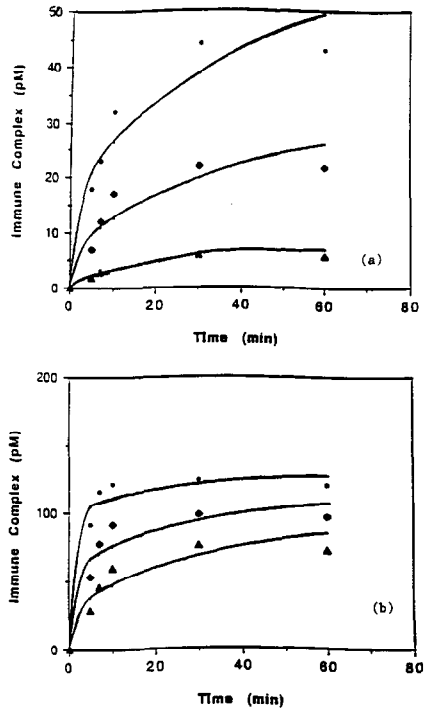

Fig. 7. Binding rate curves for human chorionic gonadotropin (hCG) to anti-hCG immobilized on a HPLC column using a liquid-phase binding assay at different hCG concentrations (in pM) [39]: (a) ▲ 11; ◆ 28; ● 55, (b) ▲ 110; ◆ 220; ● 548.

fit of the model for the non-specific binding of the antibody to the pure POPC is also shown in Fig. 6.

Table 1 indicates that the fractal dimension, D_f for the non-specific binding case is higher ($D_f = 2.3158$) as compared to the specific binding case ($D_f = 1.3391$). This is to be expected since non-specific binding would exhibit a higher state of disorder compared to specific binding. The state of disorder increases by about 72.9% as one goes from the specific binding case to the non-specific binding case. It is of interest to note that the binding rate coefficient, k_1 for the non-specific binding ($k_1 = 0.00873$) is higher (by about a factor of 2) than that of the specific binding ($k_1 = 0.004448$). However, the higher state of disorder of the non-specific binding compared to the specific binding leads to a lower amount of antibody bound to the antigen on the surface, as expected. This indicates that, in this case at least, the amount of antibody bound is rather sensitive to the state of disorder on the surface.

Note that the model as presented passes through the origin, even though the data is at 0.62 at time, t equal to zero for the specific binding case (please see Fig. 6). Once again, this is intuitively correct as far as the model is concerned. This may once again be attributed to inadequate experimental procedure leading to unreliable early time data. At least, for the specific binding case, the present model is unable to describe the full time course of the experiment. A dual-fractal analysis in this case may provide a closer fit in the initial region, but it will still not describe the data at time, t equal to zero. Once again, the present model is unable to describe the data over the full time course of the experiment.

3.3. Effect of concentration

The liquid-phase assay for human chorionic gonadotropin (hCG) using HPLC by Nakamura et al. [39] has already been analyzed with respect to changes in the temperature. Nakamura et al. [39] also determined the formation of the immune complex using different concentrations of hCG. Fig. 7a, b shows the binding curves obtained using Eq. (2) for hCG concentrations ranging from 11 to 548 pM. Table 1 indicates that the disorder on the surface increases as the hCG concentration in solution increases. The binding rate coefficient, k_1 increases by a factor of 83.5 from 1.120 to 93.51 as the hCG concentration increases by a factor of 49.8 from 11 to 548 pM.

Fig. 8 shows that the binding rate coefficient, k_1 increases linearly with increase in hCG concentration. Fig. 8 also shows that the fractal dimension, D_f increases linearly as the hCG concentration increases from 11 to about 220 pM. Around 220 pM hCG concentration the rate of increase of D_f with concentration gradually begins to decrease. This is not unexpected since the maximum value for D_f is 3. The D_f versus hCG concentration curve appears to approach this value asymptotically or exhibits the beginnings of a typical binding curve approaching equilibrium conditions.

Starodub et al. [41] have developed an optoimmunosensor for the simultaneous detection of biologically active substances in solution using a competition immunochemical analysis method. Antibodies specific to lidocaine and phenatoine labeled with fluorescein isothiocyanate (FITC) were immobilized on a fiber-optic immunosensor. Fig. 9a, b show the

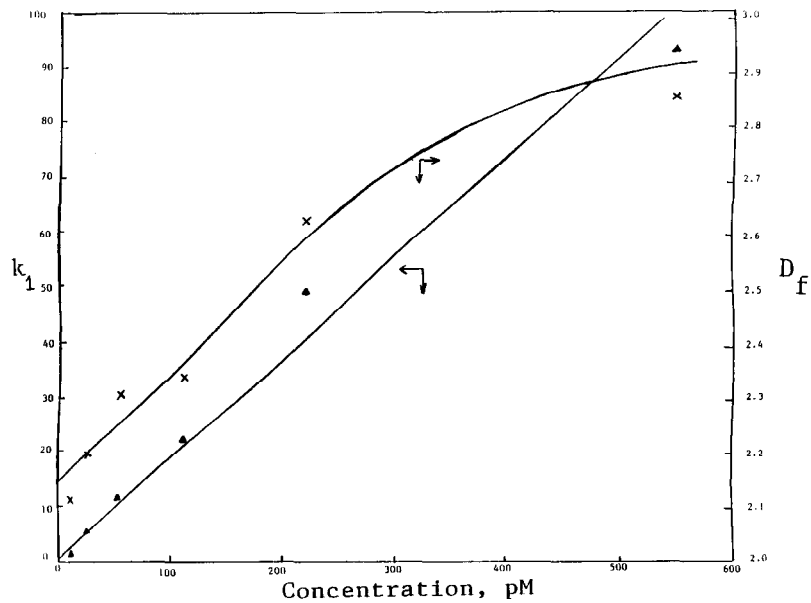

Fig. 8. Linear increase in the fractal dimension, D_f and in the binding rate coefficient, k_1 with an increase in the hCG concentration in solution for binding to anti-hCG immobilized on a HPLC column using a liquid-phase binding assay [39].

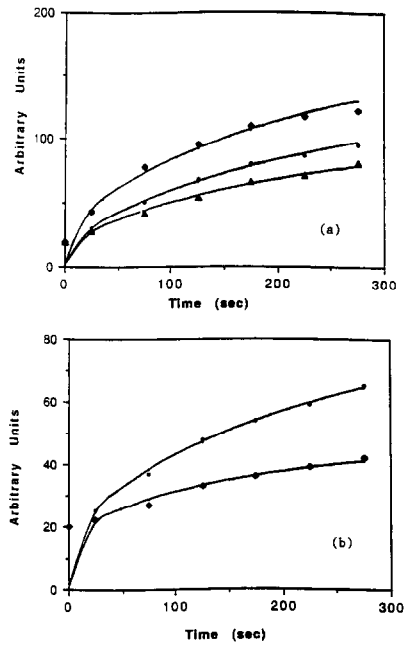

Fig. 9. Binding rate curves for phenatoine labeled with fluorescein isothiocyanate (FITC) to antibody specific to phenatoine immobilized on an immunosensor [41]. Phenatoine concentration in solution in mg ml^{-1}: (a) ◆ 0; ● 0.02; ▲ 0.2, (b) ● 2; ◆ 20.

binding curves obtained for phenatoine using Eq. (2). Table 1 shows the values of k_1, p, and D_f obtained. Once again, the model presented passes through the origin even though the data is at 20 at time, t equal to zero (please see Fig. 9a or b). This is intuitively correct as far as the model is concerned. The lack of success may once again be attributed to inadequate experimental procedure leading to unreliable early time data. No clue or method is presumably presently available from the original data to help eliminate this. Thus, the present model is unable to describe the data over the full time course of the experiment. A dual-fractal analysis would only provide a closer fit for this data point at 20 at time, t equal to zero. Even then, the model would pass through the origin, as is intuitively required.

Note that the D_f versus phenatoine concentration curve goes through a rather sharp minimum at the lower concentration (0.02 mg ml^{-1}). Please see Fig. 10. At the higher concentration, this curve exhibits linear characteristics. No explanation is offered, at present, to describe this sharp minimum exhibited. The binding rate coefficient, k_1 versus phenatoine concentration curve also exhibits characteristics simi-

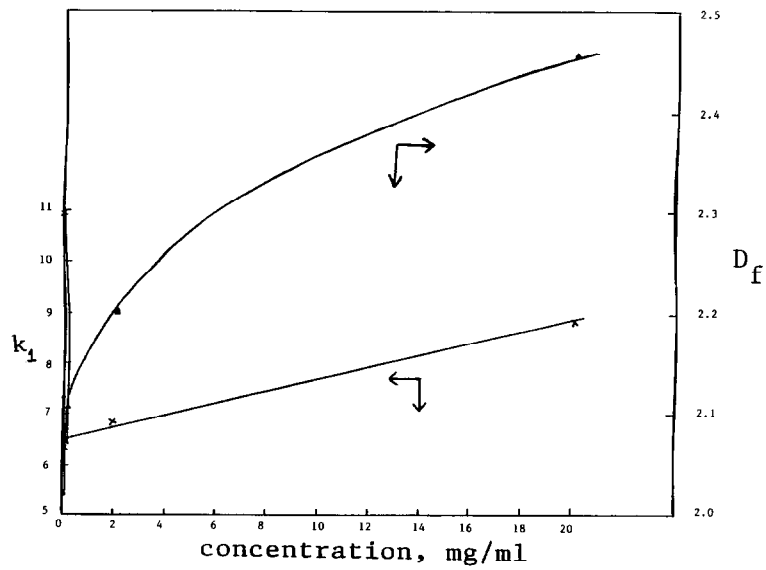

Fig. 10. Changes in the fractal dimension, D_f and in the binding rate coefficient, k_1 with changes in the phenatoine concentration in solution [41].

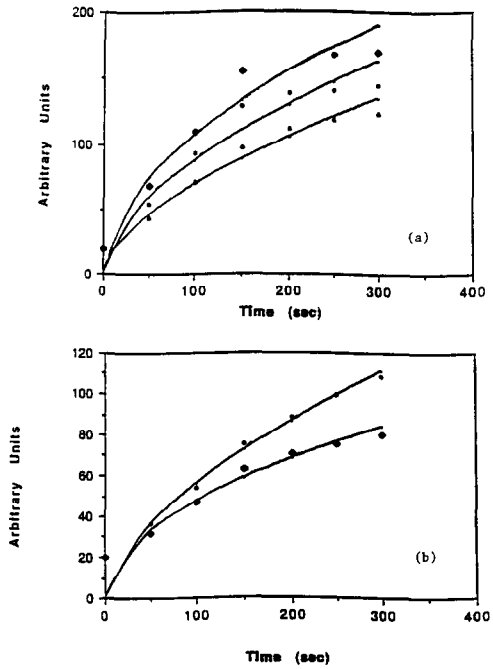

Fig. 11. Binding rate curves for lidocaine labeled with fluorescein immobilized on an immunosensor [41]. Lidocaine concentration in solution in mg ml^{-1}: (a) ♦ 0; ● 0.02; ▲ 0.2, (b) ● 2; ♦ 20.

lar to those exhibited by the D_f versus phenatoine concentration curve. Here too, at the higher phenatoine concentrations, the curve exhibits linear characteristics. It is of interest to note that the two curves mentioned above exhibit their minimum at phenatoine concentrations very close to each other.

Fig. 11a,b show the binding curves obtained for lidocaine to antibody specific to lidocaine and immobilized on a fiber-optic immunosensor using Eq. (2). Table 1 shows the values of k_1, p, and D_f obtained. Except for the data at early times, a single-fractal analysis provides an adequate fit for the lower concentrations (0 and 0.02 mg ml^{-1}) of lidocaine utilized. At the higher concentrations, a dual-fractal analysis would provide a better fit, and would help minimize the systematic deviation between the model fit and the data. Also, a dual-fractal analysis would provide a closer fit for the data point at time, t equal to zero which is located at 20. The model, even with the dual-fractal analysis would have to pass through the origin as is intuitively required. Nevertheless, as indicated before, the single-fractal model is presently unable to describe the data over the full time course of the experiment. This may partly be due to inade-

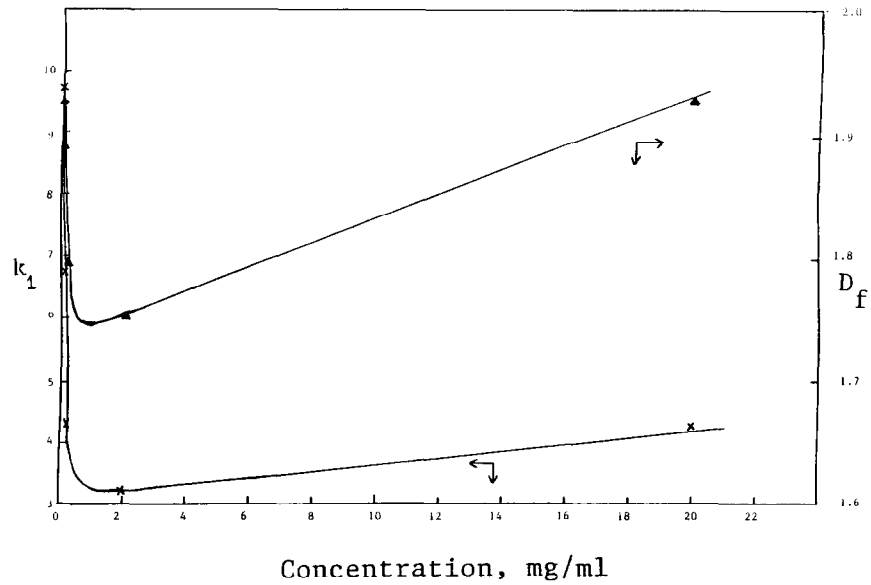

Fig. 12. Changes in the fractal dimension, D_f and in the binding rate coefficient, k_1 with changes in the lidocaine concentration in solution [41].

quate experimental procedure that leads to unreliable early time data.

The D_f versus lidocaine concentration curve exhibits a minimum at the lower concentrations (around 1 mg ml^{-1}). Please see Fig. 12. At the higher concentrations this curve exhibits linear characteristics. No explanation is offered, at present, to describe this minimum exhibited, except that similar behavior was exhibited during the detection of phenatoine. The binding rate coefficient, k_1 versus lidocaine concentration curve also exhibits characteristics similar to those exhibited by the k_1 versus phenatoine curve. Here too, at the higher lidocaine concentrations, the curve exhibits linear characteristics. Once again, the two curves for lidocaine mentioned above exhibit their minimum at lidocaine concentrations close to each other. It is of interest to note that the shapes of the D_f versus concentration and k_1 versus concentration for phenatoine and lidocaine exhibit characteristics that are similar in nature.

Wolfbeis [26] has recently analyzed the binding of different concentrations of thiamine to lipophilic anionic sites on a di-tert-butyl-0,0′-*bis*-(2,2-dichlorovinyl)-tartrate, DBVT (plasticized polymer membrane). Fig. 13a, b shows the binding curves obtained for thiamine concentration in solution ranging from 0.1 to 100 mM. Table 1 shows the values of k_1, p, and D_f obtained. Table 1 shows that as the thiamine concentration in solution increases by 3 orders of magnitude from 0.1 to 100 mM, the binding rate coefficient, k_1 increases by a factor of 90.3 from 0.02942 to 2.621, and the fractal dimension, D_f increases by a factor of 4.43 from 0.6174 to 2.7404. The low value of the fractal dimension (0.6174) at the lowest thiamine (0.1 mM) concentration utilized indicates that the surface exists as a Cantor like dust at this condition. Note that an increase in the thiamine concentration in solution leads to changes in the fractal dimension, D_f and in the binding rate coefficient, k_1 in the same direction.

The single-fractal analysis provides an adequate fit for the lowest concentration (0.1 mM) of thiamine in solution utilized. Once again, a dual-fractal analysis would provide a more refined fit for the 1 to 100 mM thiamine concentrations in solution utilized. This would help eliminate the systematic deviation for all of these four concentrations (1, 3, 10, and 100 mM). As indicated previously, the fractal dimension ob-

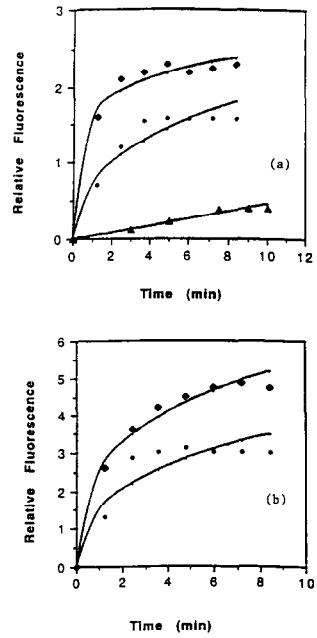

Fig. 13. Binding rate curves for thiamine in solution to lipophilic anionic sites on a di-tert-butyl-0,0′-*bis*- (2,2-dichlorovinyl)-tartrate (DBVT) plasticized polymer membrane [26]. Concentration of thiamine in solution in mM: (a) ▲ 0.1; ● 1; ◆ 3, (b) ● 10; ◆ 100.

tained at the later stages of the reaction (D_{f2}) would be higher in value than the fractal dimension value obtained during the initial stages (D_{f1}). This would also indicate that there is a change in the mechanism of binding when one compares the binding of 0.1 mM thiamine in solution with the higher thiamine concentrations (1 to 100 mM) in solution. If a dual-fractal analysis is utilized, to provide a better fit when required, then the slope of the binding curve is very small during the latter period. This leads to a relatively high value of the fractal dimension or the state of disorder on the surface. Nevertheless, the present single-fractal analysis is unable to describe the data over the full time course of the experiment. As indicated above, improvements in the fit and in physical understanding are possible by using a dual-fractal analysis.

Fig. 14 indicates that the binding rate coefficient, k_1 increases linearly with an increase in the (thiamine concentration)$^{0.25}$ in solution. The fractal dimension, D_f also exhibits an initial increase with an

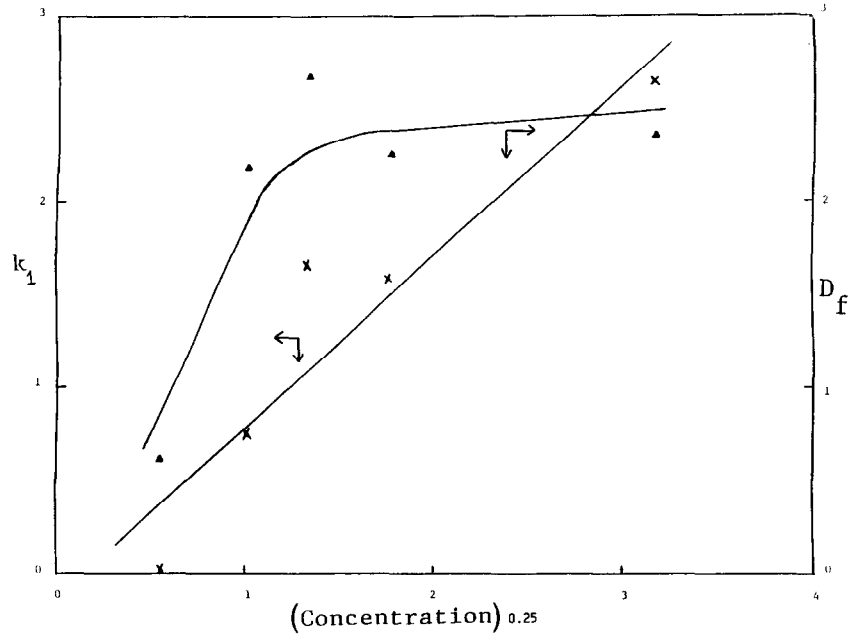

Fig. 14. Linear increase in the binding rate coefficient, k_1 and changes in the fractal dimension, D_f with an increase in the (thiamine concentration)$^{0.25}$ in solution for binding to lipophilic sites on DBVT [26].

increase in the (thiamine concentration)$^{0.25}$. At higher concentrations the D_f versus (thiamine concentration)$^{0.25}$ curve exhibits typical saturation curve characteristics. This is not unexpected, since the maximum value of D_f is 3.

Poirer et al. [42] have recently analyzed the binding of TRITC-labeled low-density lipoprotein (LDL) directly to an optical fiber-based biosensor. This is an example of ligand (protein) adsorption or binding directly to a 'receptorless' surface. Fig. 15 shows the fit of the model for the binding of TRITC-labeled low-density protein (LDL) directly to an optical fiber-based biosensor. Table 1 indicates that as the TRITC-labeled LDL concentration in solution increases by an order of magnitude from 5 to 50 μg ml^{-1} the fractal dimension, D_f decreases, and the binding rate coefficient, k_1 increases. In this case the changes in the fractal dimension, D_f and in the binding rate coefficient, k_1 are in opposite directions.

Fig. 16a shows that, in the range studied, the fractal dimension, D_f increases linearly with the reciprocal of the LDL concentration in solution. More data points would more firmly establish the trend presented. Fig. 16b shows that, in the range studied, the binding rate coefficient, k_1 increases linearly with an increase in the LDL concentration in solution. Once again, more data points would more firmly establish the trend presented. It is of interest to note that as the LDL concentration in solution increases by an order of magnitude from 5 to 50 μg ml^{-1} in solution, the fractal dimension, D_f de-

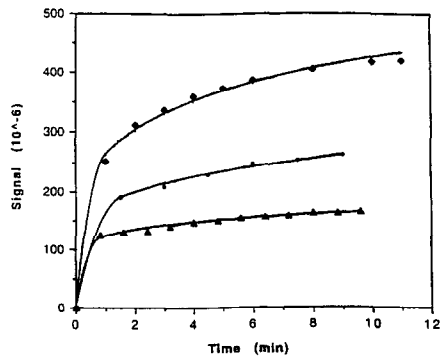

Fig. 15. Binding rate curves for TRITC-labeled low-density proteins (LDL) directly to an optical fiber-based biosensor [42]. LDL concentration in solution in μg ml^{-1}: ▲ 5; ● 10; ◆ 50.

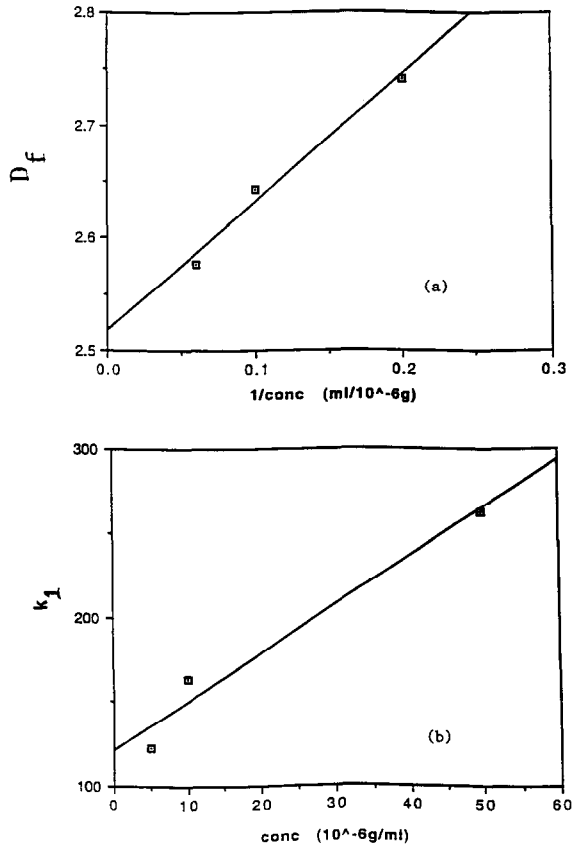

Fig. 16. (a) Linear increase in the fractal dimension, D_f with the reciprocal of the LDL concentration in solution for binding to an optical fiber-based biosensor [42]. (b) Linear increase in the binding rate coefficient, k_1 with an increase in the LDL concentration in solution [42].

creases by 5.7% from 2.7404 to 2.5829, and the binding rate coefficient, k_1 increases by a factor of 2.14 from 122.45 to 263.22.

4. Conclusions

The fractal analysis of the binding kinetics of antigen–antibody, ligand–receptor, analyte–receptorless systems for biosensor applications provides a quantitative indication of the state of disorder on the surface. The analysis presented is of a general enough nature and more-or-less the treatment applies equally well to the three systems presented. Changes in the fractal dimension, D_f observed are in the same and in the reverse directions as the forward binding rate coefficient, k_1. For example, for the binding of 2,6-TNS to β-cyclodextrin (ligand–receptor system) immobilized on a fiber-optic base inclusate biosensor, an increase in temperature from 4 to 30°C leads to an increase in the fractal dimension, D_f and to a decrease in the binding rate coefficient, k_1. For the binding of thiamine in solution to lipophilic anionic sites (receptor) on DBVT membrane, an increase in the thiamine concentration from 0.1 to 100 mM leads to increases in both the binding rate coefficient, k_1 and in the fractal dimension, D_f. Similar examples for antigen–antibody and analyte–receptorless systems are either presented here or can be readily obtained by analyzing appropriate experimental data of these types of systems available in the literature.

The present single-fractal analysis model is an initial attempt to model the binding kinetics using the fractal approach. Systematic deviations are observed during the modelling of some of the data in spite of the fact that the parameters obtained by the regression analysis [43] are within 95% confidence limits, which indicates that these values are precise and significant. Improvements in the fit may be obtained and these systematic deviations may be eliminated or minimized by utilizing a dual-fractal analysis. As presented, the single-fractal model is unable to describe the data at early times in some cases. This may be due to inadequate experimental procedure that leads to unreliable early time data. Extreme care must be exercised in analyzing this early time data, and in eliminating any possible sources that contribute to this unreliability such as a background signal, etc. Thus, the single-fractal model is unable to describe the data over the full time course of the experiment. Nevertheless, in spite of these constraints, where ever it is applicable, the model is of assistance. Further analysis and improvements in the model development are suggested.

The generalized fractal analysis treatment presented provides physical insights into the different types of binding analysis that may be utilized for biosensor applications. The present analysis represents one possible means towards the first step for a 'unified analysis' of binding reactions occurring on dispersive media for biosensor applications. A better control of the fractal dimension on the surface would significantly enhance the understanding of the sensi-

tivity, stability, selectivity, and response time of biosensors wherein different types of binding systems are utilized for analysis. Modelling coupled with experimental studies should further enhance our understanding of these and other types of binding systems that may be utilized for biosensor applications. In a more general sense, more-or-less the treatment should also be applicable to non-biosensor applications wherein further physical insights could be obtained.

References

[1] A. Seri-Levy and D. Avnir, Surf. Sci. 248 (1991) 258.
[2] M.O. Vlad, J. Colloid Interface Sci. 159 (1993) 21.
[3] T. Pajkossy and L. Nyikos, Electrochim. Acta 34 (2) (1989) 171.
[4] T. Goetze and J. Brickmann, Biophys. J. 61 (1992) 109.
[5] W.G. Glockle and T.F. Nonenmacher, Biophys. J. 68 (1995) 46.
[6] A. Sadana and A. Madagula, Biotechnol. Prog. 9 (1993) 259.
[7] A. Sadana and A. Madagula, Biosens. Bioelectron. 9 (1994) 45.
[8] A Sadana and A. Beelaram, Biotechnol. Progr. 10 (1994) 291.
[9] A. Sadana and A. Beelaram, Biosens. Bioelectron. 10 (1995) 301.
[10] M. Werthen, M. Stenberg and H. Nygren, Prog. Colloid Polymer Sci. 41 (1990) 131.
[11] M. Stenberg and H. Nygren, Biophys. Chem. 41 (1991) 131.
[12] H. Nygren, Biophys. J. 65 (1993) 1508.
[13] J.F. Douglas, H.E. Johnson and S. Granick, Science 262 (1993) 2010.
[14] A. Sadana, J.P. Alarie and T. Vo-Dinh, Talanta 42 (1995) 1567.
[15] J.A.H. Lord, A.A. Waterfield and J. Hughes, Nature (London) 267 (1977) 495.
[16] H. Eriksson, S. Upchurch, J.W. Hardin, E.J. Peck, Jr. and J.H. Clark, Biochem. Biophys. Res. Commun. 81 (1978) 1.
[17] M.K. Agarwal and M. Phillipe, Biochim. Biophys. Acta 500 (1977) 42.
[18] D.B. Barnett, E.L. Rugg and S.R. Nahorski, Nature (London) 273 (1978) 166.
[19] M.V. Jose, Anal. Biochem. 144 (1985) 494.
[20] M.V. Jose and C. Larralde, Math. Biosci. 58 (1982) 159.
[21] J.D. Swalen, J. Allara, J.D. Andrade, E.A. Chandross, S. Garoff, J. Israelachvili, T.J. McCarthy, R. Murray, R.F. Pease, J.F. Rabolt, K.J. Wynne and H. Yu, Langmuir 3 (1987) 932.
[22] R.C. Ebersole, J.A. Miller, J.R. Moran and M.D. Ward, Biophys. J. 59 (1990) 387.
[23] M. Losche, M. Pieponstock, A. Diederich, T. Gruneweld, K. Kjaer and D. Vaknin, Biophys. J. 65 (1993) 2160.
[24] D. Axelrod and M.D. Wang, Biophys. J. 64 (1994) 588.
[25] A. Sadana and D. Sii, Biosens. Bioelectron. 7 (1992) 559.
[26] O.S. Wolfbeis, Anal. Chim. Acta 250 (1991) 181.
[27] R. Kopelman, Science 241 (1988) 1620.
[28] E. Di Cera, J. Chem. Phys. 95 (1991) 5082.
[29] A. Sadana and D. Sii, J. Colloid Interf. Sci. 151(1) (1992) 166.
[30] P.A. Cuypers, G.M. Willems, J.M. Kop, J.W. Corsel, M.P. Jansen and W.T. Hermens, in J.L. Brash and T.A. Horbett (Editors), Proteins At Interfaces. Physicochemical And Biochemical Studies (American Chemical Society, Washington, D.C., 1987) pp. 208–211.
[31] A. Sadana, Biotechnol. Progr. 11 (1995) 50.
[32] J. Anderson, NIH Panel Review Meeting, Case Western Reserve University, Cleveland, OH, July 1993.
[33] P.G. De Gennes, Radiat. Phys. Chem. 22 (1982) 193.
[34] P. Pfeifer, D. Avnir and D.J. Farin, Nature (London) 308 (5956) (1984) 261.
[35] P. Pfeifer, D. Avnir and D.J. Farin, J. Colloid Interf. Sci. 103 (1) (1984) 112.
[36] L. Nyikos and T. Pajkossy, Electrochim. Acta 31 (1986) 1347.
[37] S. Havlin, in D. Avnir (Editor), The Fractal Approach To Heterogeneous Chemistry: Surfaces, Colloids, Polymers (Wiley, New York, 1989) pp. 251–269.
[38] K.S. Litwiler, G.C. Catena and F.V. Bright, Anal. Chim. Acta 237 (1990) 485.
[39] K. Nakamura, S. Satomura and S. Matsuura, Anal. Chem. 65 (1993) 613.
[40] M. Ahlers, D.W. Grainger, J.N. Herron, K. Lim, H. Ringsdorf and C. Salesse, Biophys. J. 63 (1992) 823.
[41] N.F. Starodub, P.Ya. Arenkov, A.E. Rachkov and V.A. Berezin, Sensors Actuators B 13–14 (1993) 728.
[42] M.A. Poirer, T. Lopes and B.R. Singh, Appl. Spectrosc. 48 (7) (1994) 867.
[43] Sigmaplot, Scientific Graphing Software, User's Manual, Jandel Scientific, San Rafael, CA, 1993.
[44] M.C. Cross and P.C. Hohenberg, Science 263 (1994) 1569.